Local Bit-plane Decoded Pattern: A Novel Feature Descriptor for Biomedical Image Retrieval

Shiv Ram Dubey, *Student Member*, *IEEE*, Satish Kumar Singh, *Senior Member*, *IEEE*, and Rajat Kumar Singh, *Senior Member*, *IEEE*

***Abstract*— A novel image feature descriptor based on local bit-plane decoded pattern (LBDP) is introduced for indexing and retrieval of biomedical images in this paper. A local bit-plane transformation scheme is proposed to compute the local bit-plane transformed values for each image pixel from the bit-plane binary contents of its each neighboring pixels. The introduced LBDP is generated by finding a binary pattern using the difference of centre pixel's intensity value with the local bit-plane transformed values. The efficacy of LBDP is tested under biomedical image retrieval using average retrieval precision and average retrieval rate. Three benchmark databases Emphysema-CT, NEMA-CT and OASIS-MRI are used for the evaluation and comparison of the proposed approach with recent state-of-art methods. The experimental results confirm the discriminative ability and the efficiency of the proposed LBDP for biomedical image indexing and retrieval and prove the outperformance of existing biomedical image retrieval approaches.**

***Index Terms*—Local features, biomedical image, image retrieval, local bit-plane transformation, LBP, LTP.**

I. INTRODUCTION

THE patient diagnosis in medical institutions and hospitals is becoming more challenging day by day due to hasty growth of biomedical images. X-ray, ultrasound (US), magnetic resonance imaging (MRI), computer tomography (CT), etc. are the common formats of the patient diagnosis database images. The biomedical data should be structured to allow the efficient search, access and retrieval in order to facilitate the automatic decision support patient diagnosis using expert systems. Content-based biomedical image indexing and retrieval is turning up continuously to combat this problem on the basis of the visual cues representation of the image such as color, texture, shape, structure, faces etc. Using biomedical image retrieval, the physician can point out the disorder present in the patient report by retrieving the most similar report from related reference reports. The existing biomedical image retrieval systems are depicted through published literature [1]-[7].

The feature extraction step is the backbone of any retrieval system and its efficiency is heavily dependent upon the ways of extracting features from images. The extensive and comprehensive literature survey on CBIR is reported through published literature [8]-[10]. Texture analysis has shown a stamp in solving the pattern recognition and computer vision problems because it captures the fine details of the image very efficiently [11]-[12]. Texture based biomedical image retrieval is excellently suited to retrieve the type of the diseases present in the image which make it more popular for medical perspective [13]-[16]. It can be seen as an instance of the texture based image retrieval which is widely adopted in retrieval research community. Some recent methods designed for biomedical image retrieval are depicted in [17]-[19]. A local diagonal extrema pattern based on the center pixel and local diagonal neighbors is proposed in [17] for CT image retrieval. In [18], the image features are described using local ternary co-occurrence pattern for MRI and CT image retrieval. In [19], binary wavelet patterns in multiple directions are proposed for biomedical retrieval application. To reduce the memory required for image storage, physiological kinetic feature is presented by Cai et al. [20] for positron-emission-tomography (PET) image retrieval.

Ojala et al. [11] introduced the local binary pattern (LBP) for texture classification. LBP operator became more popular due to its reduced computational complexity. Several other LBP variants [12], [21]-[23] also came into existence in view of high success of LBP in different applications such as in face recognition [24], analysis of facial paralysis [25], analysis of pulmonary emphysema [26], etc. Local ternary pattern is proposed as the generalization of LBP for face recognition under changing lighting conditions [27]. Centre symmetric local binary pattern is investigated to reduce the dimension of the LBP for local region matching [28]. Dubey et al. presented an illumination compensation mechanism to cope with brightness change [29]. Recently, they also combined the local intensity orders in an interleaved fashion for feature description [30]. Peng et al. extracted the texture cues in chest CT images on the basis of the uniformity of structure and brightness in the image [31]. They depicted the structure and brightness in the image using extended rotation invariant local binary pattern and difference in gradient orientations. Region of interest retrieval is proposed by Unay et al. [32] in brain MR images on the basis of the local structure exist in the image. SVM-based feature selection is applied over the textural features for tumor recognition [33] in wireless capsule endoscopy images. Local Mesh Patterns (LMeP) [34], Peak Valley Edge Patterns (PVEP) [35] and local mesh peak valley edge patterns [36] are the latest state-of-art descriptors proposed for the biomedical image retrieval.

The local feature descriptions presented through the published literature have utilized the relationship of a referenced pixel with its neighboring pixel. The performance of such descriptors improved but at the expense of increased image matching time because its dimension is very high which increases the retrieval time complexity. This is the motivation

The authors are with the Indian Institute of Information Technology, Allahabad, India (shivram1987@gmail.com, sk.singh@iiita.ac.in, rajatsingh@iiita.ac.in).

The final paper DOI: http://dx.doi.org/10.1109/JBHI.2015.2437396

for us to propose a novel low dimensional and time efficient local bit-plane decoded pattern (LBDP). The performance of the proposed method is also improved. The LBDP encodes the relationship among neighbors in each bit-plane separately using local bit-plane transformation which generates the local bit-plane transformed values and then encodes the relationship of centre pixel with each transformed values. The efficacy of proposed approach has been made confirmed through three biomedical image retrieval experiments.

This manuscript is integrated in following manner. Section II presents the proposed framework for biomedical image indexing and retrieval and also proposed the LBDP feature vector. Section III describes the evaluation criteria. In Section IV, experimental results are presented with discussions and finally concluding remarks are highlighted in Section V.

II. Proposed Biomedical Image Retrieval Framework

In this section, we proposed the framework for biomedical image retrieval using local bit-plane decoded pattern ($LBDP$). Fig. 1 presents the steps involved in biomedical image retrieval framework. Local bit-plane decomposition, local bit-plane transformation, local bit-plane decoded pattern, local bit-plane decoded feature vector and similarity measurement are the main components of the introduced framework. In rest of this section, we describe each component in detail.

A. Local Bit-plane Decomposition

In contrast with the existing local feature descriptors we have not used the intensity values of the local neighbors of any referenced pixel as it. We decomposed these values into local bit-planes for further processing. Let M is a grayscale image of dimension $m_1 \times m_2$ with bit depth of B-bit. The $P^{i,j}$ is the pixel of image M at coordinate (i,j) in Cartesian coordinate system and $I^{i,j}$ is the intensity value of pixel $P^{i,j}$. The N local neighbors of $P^{i,j}$ evenly distributed at a circle of radius R having centre at $P^{i,j}$ are represented by a set $P^{i,j}_{R,N}$. As depicted in Fig. 2, the t^{th} neighbor of $P^{i,j}$ (i.e. t^{th} element of $P^{i,j}_{R,N}$) is denoted as $P^{i,j}_{R,N,t}$ having intensity value $I^{i,j}_{R,N,t}$ where t is positive integer and $t \in [1,N]$.

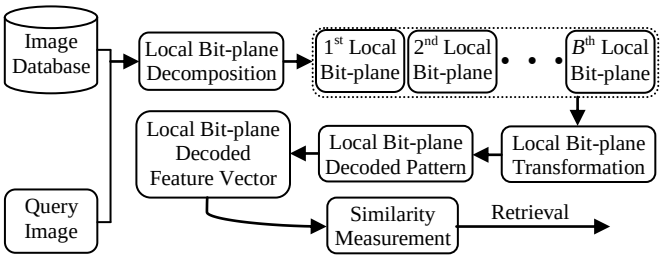

Fig. 1. Proposed system framework for biomedical image retrieval.

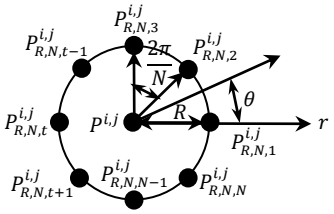

Fig. 2. The local neighbors of a centre pixel in polar coordinate system.

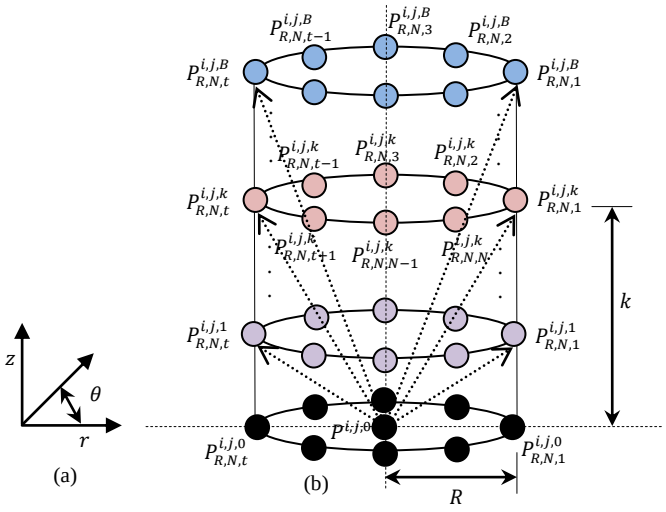

Fig. 3. (a) Cylindrical coordinate system axis, (b) the local bit-plane decomposition. The cylinder can be think of the B + 1 horizontal slices. The base slice of the cylinder is composed of the original centre pixel and its neighbors with the centre pixel at the origin. The remaining B slices correspond to the B bit-planes of the local neighbors of base slice. The $(t+1)^{th}$ slice from the base corresponds to the t^{th} bit-plane of the base slice.

The coordinate of $P^{i,j}_{R,N,t}$ with respect to the origin in Cartesian coordinate (x,y) is given as,

$$x(P^{i,j}_{R,N,t}) = i - r(P^{i,j}_{R,N,t}) \times sin(\theta(P^{i,j}_{R,N,t})) \quad (1)$$

$$y(P^{i,j}_{R,N,t}) = j + r(P^{i,j}_{R,N,t}) \times cos(\theta(P^{i,j}_{R,N,t})) \quad (2)$$

where $r(P^{i,j}_{R,N,t})$ and $\theta(P^{i,j}_{R,N,t})$ is the coordinate of $P^{i,j}_{R,N,t}$ in the polar coordinate system w.r.t. the $P^{i,j}$ and computed as,

$$r(P^{i,j}_{R,N,t}) = R \quad (3)$$

$$\theta(P^{i,j}_{R,N,t}) = (t-1) \times \frac{2\pi}{N} \quad (4)$$

The local bit-plane decomposition step is performed to separate each bit-plane k of the local neighboring structure of the pixel $P^{i,j}$, where k is the positive integer with $k \in [1,B]$. The local bit-plane decomposition step yields the binary values in each bit-plane and applied over only neighbors $P^{i,j}_{R,N}$. Note that this step is not applied over the centre pixel $P^{i,j}$. It would be more useful and interesting if each bit-plane is represented in cylindrical coordinate system because this coordinate system can be easily demonstrated with the help of polar coordinate system. We represent the elements of the bit-planes in the cylindrical coordinate system (r, θ, z) as shown in Fig. 3 where r and θ can be used to find the spatial coordinate in the polar coordinate system and z can be used to find the bit-plane number. The cylinder is composed of the $B+1$ stacked horizontal slices, where the base slice represents the original $N+1$ pixels (i.e. one centre pixel and N its neighbors). The original centre pixel $P^{i,j}$ becomes the origin of the cylindrical coordinate system and represented by $P^{i,j,0}$ because $z(P^{i,j,0}) = 0$. The B bit-planes of the neighbors $P^{i,j}_{R,N}$ are contained by the remaining B slices of the cylinder with B^{th} bit-plane at the top of the cylinder. The notation in polar coordinate of t^{th} neighbor (i.e. $P^{i,j}_{R,N,t}$) is changed to $P^{i,j,0}_{R,N,t}$ in the cylindrical coordinate because they are contained

by the base of the cylinder. Let $P_{R,N,t}^{i,j,k}$ represents the element corresponding to $P_{R,N,t}^{i,j,0}$ in k^{th} bit-plane for $\forall\, k \in [1,B]$ and $\forall\, t \in [1,N]$ and its binary value is denoted by $I_{R,N,t}^{i,j,k}$. The r, θ, and z coordinates of t^{th} element (i.e. corresponding to the t^{th} neighbor of $P^{i,j,0}$) in k^{th} bit-plane are given as,

$$r(P_{R,N,t}^{i,j,k}) = R \tag{5}$$

$$\theta(P_{R,N,t}^{i,j,k}) = (t-1) \times \frac{2\pi}{N} \tag{6}$$

$$z(P_{R,N,t}^{i,j,k}) = k \tag{7}$$

The binary value $I_{R,N,t}^{i,j,k}$ of t^{th} neighbor of $P^{i,j,0}$ in k^{th} bit-plane is defined from intensity value of $P_{R,N,t}^{i,j,0}$ (i.e. $I_{R,N,t}^{i,j,0}$) as,

$$I_{R,N,t}^{i,j,k} = \left\lfloor \frac{f^k}{2} \right\rfloor - \left\lfloor \frac{f^k}{2} \right\rfloor \tag{8}$$

$$f^k = \begin{cases} I_{R,N,t}^{i,j,0} & ,if\ k = 1 \\ \left\lfloor \dfrac{f^{k-1}}{2} \right\rfloor & ,otherwise \end{cases} \tag{9}$$

If $I_{R,N,t}^{i,j,k}$ is the binary value in k^{th} bit-plane for $k \in [1,B]$ corresponding to the intensity value $I_{R,N,t}^{i,j,0}$ then $I_{R,N,t}^{i,j,0}$ can be computed back using following equation,

$$I_{R,N,t}^{i,j,0} = \sum_{k=1}^{B} \tilde{I}_{R,N,t}^{i,j,k} \quad \forall\, t \in [1,N] \tag{10}$$

where $\tilde{I}_{R,N,t}^{i,j,k}$ is the weighted value of t^{th} neighbor in k^{th} bit-plane and computed using following equation,

$$\tilde{I}_{R,N,t}^{i,j,k} = I_{R,N,t}^{i,j,k} \times w_1^k \tag{11}$$

where w_1^k is a weight value for any element of k^{th} bit-plane and defined as follows,

$$w_1^k = (2)^{(k-1)} \tag{12}$$

The local bit-plane decomposition is illustrated using an example pattern in Fig. 4 for $R = 1$, $N = 8$ and $B = 8$. The example pattern shown in Fig. 4(a) comprises of a centre pixel and its 8 neighbors. The 8 bit-planes consisting of the binary values for each neighbor are depicted in Fig. 4(b) with the help of circles of two colors. The 'red' and 'green' color circles stand for '1' and '0' respectively. The neighbors of the sample pattern can be computed back from the bit-planes using (10). So, finally after the local bit-plane decomposition step, we generated the binary values $I_{R,N,t}^{i,j,k}$ for $\forall\, k \in [1,B]$ and $\forall\, t \in [1,N]$ which is going to be used by the next step.

B. *Local Bit-plane Transformation*

The local binary pattern [11] uses the raw intensity values of neighboring pixels without any transformation which became motivation for us to introduce a concept of local bit-plane transformation which captures the local information in each bit-plane separately with lower and higher bit-plane capture the fine and coarse details respectively. The local bit-plane transformed values for each bit-plane are generated using this transformation. The local bit-plane transformed value for k^{th} bit-plane (i.e. $v_{R,N}^{i,j,k}$) using the decomposed value of each neighbor in k^{th} bit-plane is defined as,

$$v_{R,N}^{i,j,k} = \sum_{t=1}^{N} \bar{\bar{I}}_{R,N,t}^{i,j,k} \tag{13}$$

where $k \in [1,B]$ and $\bar{\bar{I}}_{R,N,t}^{i,j,k}$ is the weighted value of t^{th} neighbor in k^{th} bit-plane and computed as,

$$\bar{\bar{I}}_{R,N,t}^{i,j,k} = I_{R,N,t}^{i,j,k} \times w_2^t \tag{14}$$

where w_2^t is a weighting factor for t^{th} neighbor in any bit-plane and computed as follows,

$$w_2^t = (2)^{(t-1)} \tag{15}$$

The local bit-plane transformed values for a particular bit-plane is computed by summing each weighted values using w_2 in that bit-plane. Note that weight w_2 is defined for each neighbor over a particular bit-plane whereas weight w_1 is defined for each bit-plane of a particular neighbor.

It should also be noted that the number of N neighboring values are transformed into B values. The range of $v_{R,N}^{i,j,k}$ is between 0 and 2^{N-1} (i.e. $v_{R,N}^{i,j,k} \in [0, 2^{N-1}]$). Now we have B local bit-plane transformed values which are further used along with the original intensity value of centre pixel to generate a local bit-plane decoded pattern for the centre pixel $P^{i,j,0}$. The local bit-plane transformed values for the local bit-planes of Fig. 4(b) using the weight w_2 are computed as 244, 239, 98, 8, 33, 164, 71 and 0 for bit-plane number $k = 1$ to 8 respectively. We considered an example image in Fig. 5(a) to show the characteristics of introduced local bit-plane transformation. Fig. 5(b) portrayed the LBP map [12] computed over considered image. The local bit-plane transformed values maps is displayed in Fig. 5(c-j) for bit-plane number $k = 1$ to 8 respectively; these maps are generated for $N = 8$ and $p = 8$. It is observed from Fig. 5 that LBP is not able to encode very fine details of the image which is encoded by the lower bit-planes of the local bit-plane transformation scheme. It is also deduced that the lower bit-plane maps capture more fine details whereas the higher bit-plane maps catch the more coarse details.

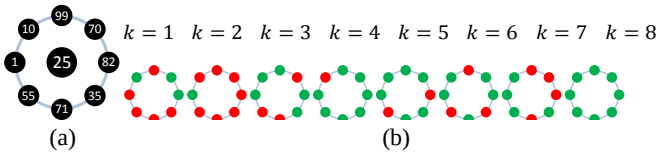

Fig. 4. An example of bit-plane decomposition into $B = 8$ bit-planes, (a) A sample pattern with $R = 1$ and $N = 8$, (b) The decomposed bit-planes of the neighbors; the 'red' and 'green' circles represent '1' and '0' respectively.

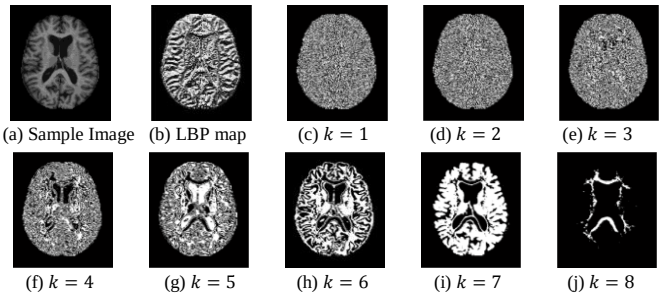

Fig. 5. Example of local bit-plane transformed values map for each bit-planes for $N = 8$ and $B = 8$, (a) sample image, (b) LBP map over sample image, (c-j) local bit-plane transformed value maps for each bit-plane.

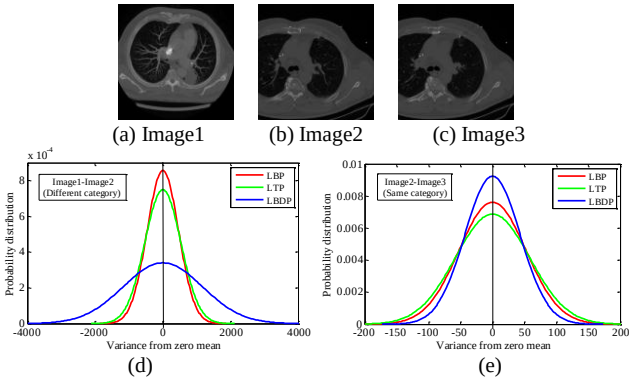

Fig. 6. Examples illustrating the behavior of LBP, LTP and LBDP for inter and intra class images; (a, b, c) Image1, Image2 and Image3 respectively are three images where first two are from different classes and last two are from the same classes, (d-e) The probability distributions of absolute difference of the feature vectors of each method w.r.t. the zero mean for inter (Image1 and Image2) and intra (Image2 and Image3) class images respectively.

C. Local Bit-plane Decoded Pattern

In this subsection, we utilize the concept of local bit-plane transformation to generate a binary pattern called as local bit-plane decoded pattern ($LBDP$) by exploring the relation between intensity value $I^{i,j,0}$ of a centre pixel $P^{i,j,0}$ with the local bit-plane transformed values $v_{R,N}^{i,j,k}$ for each bit-plane $k \in [1, B]$. The $LBDP$ pattern for pixel $P^{i,j}$ of image M using N neighbors at radius R is given by concatenating the $LBDP_{R,N}^{i,j,k}$ values for each $k \in [1, B]$ as follows,

$$LBDP_{R,N}^{i,j} = \{LBDP_{R,N}^{i,j,1}, LBDP_{R,N}^{i,j,2}, \dots\dots\dots, LBDP_{R,N}^{i,j,B}\} \quad (16)$$

where $LBDP_{R,N}^{i,j,k}$ is a binary LBDP pattern value computed over k^{th} bit-plane as,

$$LBDP_{R,N}^{i,j,k} = sign(\Delta_{R,N}^{i,j,k}) \quad (17)$$

where, $sign(\alpha)$ is a sign function and can be calculated as,

$$sign(\alpha) = \begin{cases} 1, & if\ \alpha > 0 \\ 0, & Otherwise \end{cases} \quad (18)$$

and $\Delta_{R,N}^{i,j,k}$ is the local bit-plane transformed difference computed for k^{th} bit-plane by taking the difference of $I^{i,j,0}$ from $\hat{v}_{R,N}^{i,j,k}$. The $\Delta_{R,N}^{i,j,k}$ for k^{th} bit-plane is defined as,

$$\Delta_{R,N}^{i,j,k} = \hat{v}_{R,N}^{i,j,k} - I^{i,j} \quad (19)$$

where $k \in [1, B]$ and $\hat{v}_{R,N}^{i,j,k}$ is a value obtained after range matching of $v_{R,N}^{i,j,k}$ and defined as follows,

$$\hat{v}_{R,N}^{i,j,k} = \left\lfloor \frac{v_{R,N}^{i,j,k} + 1}{2^{(N-B)}} \right\rfloor - 1 \quad (20)$$

Note that the range of $v_{R,N}^{i,j,k}$ is between 0 and 2^{N-1} whereas the range of $I^{i,j,0}$ is between 0 and 2^{B-1}. We need to match the range of $v_{R,N}^{i,j,k}$ with the range of $I^{i,j,0}$. We obtained $\hat{v}_{R,N}^{i,j,k}$ after the range matching of $v_{R,N}^{i,j,k}$ with $I^{i,j,0}$ by dividing $v_{R,N}^{i,j,k}$ with the range matching factor $2^{(N-B)}$. For the case when number of local neighbors is equal to the number of bit-planes (i.e. $N = B$), the range matching factor becomes '1' or in other word for this case range matching is not needed. Thus, $LBDP$ binary pattern is generated of length B. The value of both N and B are considered as 8 in the example of Fig. 4 so for this example range matching is not required. The local bit-plane transformed difference values are computed as 219, 214, 73, -17, 8, 139, 46, and -25 for bit-plane number $k = 1$ to 8 respectively by subtracting centre pixel's intensity value 25 from the local bit-plane transformed values 244, 239, 98, 8, 33, 164, 71 and 0 respectively generated in the previous subsection. According to the sign of the computed local bit-plane transformed difference values, the $LBDP$ pattern of centre pixel of the example considered is '11101110'.

D. Local Bit-plane Decoded Feature Vector

We generated the local bit-plane decoded patterns ($LBDP$) in previous subsection using proposed local bit-plane transformation scheme. The $LBDP$ values are computed in the binary form for a particular pixel which needs to be converted into the form of histogram. The local bit-plane decoded feature vector ($\mathcal{H}$) of 2^B dimension is calculated using the $LBDP$s of every pixels of image M. We find the $\mathcal{H}_{R,N}$ using the following equation when N neighbors evenly distributed at a circle of radius R are used to generate the patterns,

$$\mathcal{H}_{R,N}(\zeta) = \sum_{i=1}^{m_1}\sum_{j=1}^{m_2} f_1(\Im_{R,N}^{i,j}, \zeta) \quad (21)$$

for $\forall\ \zeta \in [0, 2^B - 1]$, where, $f_1(\beta, \gamma)$ is given as,

$$f_1(\beta, \gamma) = \begin{cases} 1, & if\ \beta = \gamma \\ 0, & Otherwise \end{cases} \quad (22)$$

and $\Im_{R,N}^{i,j}$ is the local bit-plane decoded value computed as,

$$\Im_{R,N}^{i,j} = \sum_{k=1}^{B} LBDP_{R,N}^{i,j,k} \times {w_1}^k \quad (23)$$

where ${w_1}^k$ is a weighting factor for k^{th} bit-plane defined in (12) and $LBDP_{R,N}^{i,j,k}$ is the local bit-plane decoded pattern value for pixel (i, j) in k^{th} bit-plane and computed using (17).

We compared the LBP [12], LTP [27] and LBDP feature vectors using images of inter and intra categories in Fig. 6. Fig. 6(a-c) show three images Image1, Image2 and Image3 respectively; Note that Image1 and Image2 are from different categories whereas Image2 and Image3 are from the same category. Fig. 6(d-e) illustrate the probability distributions of absolute difference of the feature vectors using each method w.r.t. the zero mean for inter (Image1 and Image2) and intra (Image2 and Image3) class images respectively. The x-axis shows the deviation from the zero mean and y-axis shows the probability that the feature vector of one image differs from another by a particular amount of deviation. The large amplitude of probability at zero mean signifies the high similarity between the feature vectors whereas more deviation from zero mean represent the less similar feature vectors. This figure is evident that LBDP feature vector better differentiates inter images and better matches intra images.

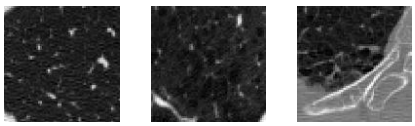

Fig. 7. Images from Emphysema-CT database, one image from each class.

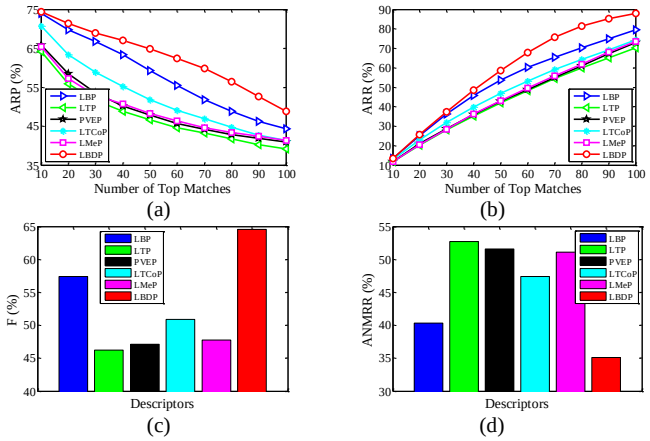

Fig. 8. Results over Emphysema-CT database for different descriptor using (a) ARP, (b) ARR, (c) F-score and (d) ANMRR evaluation criteria.

III. Evaluation Criteria

In evaluation, each image of the database db is considered as a query image in all experiments conducted in this paper. The system retrieves t_m top matches database images for each query image using shortest image matching distances by d_1 similarity measures using [18] [35] [36]. We adopted d_1 distance measure in this paper such that a fair comparison can be made between different features because most of the other methods considered in this paper for comparison purpose also have used $d1$ similarity metric in their source papers. The d_1 similarity between the features $\mathcal{H}^{q_1}$ and $\mathcal{H}^{q_2}$ of dimension dim of two images q_1 and q_2 respectively is defined as,

$$d_1(q_1, q_2) = \sum_{\lambda=1}^{dim} \left| \frac{\mathcal{H}^{q_1}(\lambda) - \mathcal{H}^{q_2}(\lambda)}{1 + \mathcal{H}^{q_1}(\lambda) + \mathcal{H}^{q_2}(\lambda)} \right| \quad (24)$$

In this paper, we have turned all the images of the database as the query image and retrieved the t_m top matching images. The system matches those retrieved images correctly which are retrieved from the same category as of the query image. We computed the average retrieval precision (ARP), average retrieval rate (ARR), F-score (F) and average normalized modified retrieval rank as the functions of the number retrieved images (t_m) in all the experiments as the performance matrices. We computed the ARP and ARR by measuring the means of the average precision and average recall respectively over each class of the database. Average precision and average recall for a class is computed by measuring the means of the precision and recall respectively by turning each image of that class as the query image. The precision and recall for any query image (M_q) is given as,

$$Precision = \frac{Number\ of\ relevent\ images\ retrieved}{Number\ of\ images\ retrieved\ (t\_m)} \quad (25)$$

$$Recall = \frac{Number\ of\ relevent\ images\ retrieved}{Number\ of\ relevent\ images\ in\ the\ db} \quad (26)$$

In order to measure the F-measure (F) metric, we have retrieved the $max(t\_m)$ number of images, where $max(t\_m)$ is the maximum number of images in any class of the database. The F-measure is given as follows,

$$F = \frac{2 \times ARP \times ARR}{ARP + ARR} \quad (27)$$

Table 1. The improvement (%) in the performance by LBDP over LBP, LTP, PVEP, LTCoP and LMeP descriptors in terms of the ARP for $t\_m = 50$, ARR for $t\_m = 100$, F and ANMRR over Emphysema-CT database

In terms of the	The performance gain of LBDP in % as compared to				
	LBP	LTP	PVEP	LTCoP	LMeP
ARP for $t\_m = 50$	09.27	39.03	35.29	25.01	34.31
ARR $t\_m = 100$	10.41	25.15	20.13	18.22	19.28
F	12.42	39.70	36.91	26.75	35.11
ANMRR	12.90	33.39	31.92	25.96	31.32

Table 2. Categorical performance comparison of different methods in terms of the Average Precision for $t\_m = 50$ over Emphysema-CT database

Category	Method					
	LBP	LTP	PVEP	LTCoP	LMeP	LBDP
NE	47.90	42.68	53.63	47.66	55.63	46.81
CLE	67.36	50.00	42.96	57.20	43.84	71.60
PSE	62.75	47.22	47.19	50.71	45.36	76.07
Average	59.33	46.63	47.92	51.86	48.27	64.83

In order to find out the average normalized modified retrieval rank (ANMRR) metric, we have used the algorithm given in [37] and represented the ANMRR in the percentage. The higher value of ARP, ARR and F represents the better retrieval performance and vice-versa, whereas the lower value of ANMRR means the better retrieval result and vice-versa.

IV. Results and Observations

In this section, we evaluate the proposed retrieval system for three biomedical image indexing and retrieval experiments using ARP and ARR values. The three experiments are performed over Emphysema-CT [38], NEMA-CT [39], and OASIS-MRI [40] databases respectively. The MRI images are available after preprocessing such as noise removal [41]. In the following subsection, we discussed the results obtained for each experiment. We have considered 8 local neighbors (N) equally spaced at a radius (R) of 1 centered at the centre pixel with 8 bit-planes (B) to construct the LBDP feature descriptor. These values are used in all experiments until or otherwise specified. We compare the results of the LBDP with the results of the LBP [12], LTP [27], PVEP [35], LTCoP [18] and LMeP [34] methods in each experiment below.

A. *Experiment #1*

The loss of lung tissue is identified as the Emphysema. In order to analyze the Emphysema disease in more details, it is crucial to recognize the healthy and emphysematous lung tissues. We have used the CT images of the Emphysema disease named as the Emphysema-CT database [38]. The Emphysema-CT database comprises of the 3 classes namely, Normal Tissue (NT), Centrilobular Emphysema (CLE), and Paraseptal Emphysema (PSE) with 59, 50 and 59 images respectively composed from the 39 persons [38]. We described the emphysema morphology by featuring the Emphysema-CT image with the help of texture based descriptors and analyzed the retrieval results over the Emphysema-CT database. Fig. 7 displayed one example images from each category. Fig. 8 illustrates the performance using ARP (%), ARR (%), F (%) and ANMRR (%) of introduced as well as other approaches over Emphysema-CT database. LBDP performs better than the remaining descriptor

as depicted in Fig. 8. Table 1 summarizes the % improvement caused by the LBDP over LBP, LTP, PVEP, LTCoP and LMeP descriptors in terms of the ARP for $t\_m = 50$, ARR for $t\_m = 100$, F and ANMRR over Emphysema-CT database. It is clear from this table that the LBDP has highest and lowest gains against the LTP and LBP descriptors respectively. Table 2 depicts the categorical performance comparison among the descriptors when $t\_m = 50$ in terms of the average precision. The LBDP descriptor performs better for the emphysematous lung tissues (i.e. for CLE and PSE class). We deduced from the results that the proposed method outperforms the existing methods over Emphysema-CT database.

B. *Experiment #2*

The National Electrical Manufacturers Association (NEMA) [39] created the digital imaging and communications in medicine (DICOM) standard to facilitate the storage and uses of medical images for research purpose. We considered the CT0001, CT0003, CT0020, CT0057, CT0060, CT0080, CT0082, and CT0083 cases of this database for experiments. We considered the 499 CT images (same images are used in [17]) of resolution 512×512 taken from the different body parts of NEMA in this study and classified it into 8 different classes (each class for different body parts) which consists of the 104, 46, 29, 71, 108, 39, 33 and 69 images to form the NEMA-CT database. Four sample images from each class of NEMA-CT database is displayed in Fig. 9.

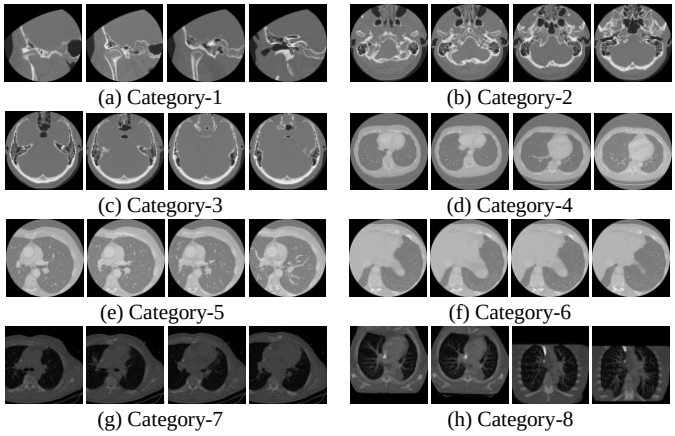

Fig. 9. Sample images from each category of the NEMA-CT database.

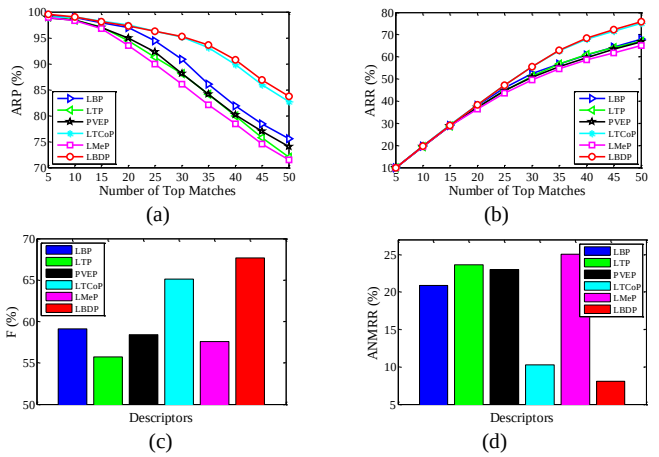

Fig. 10. Results comparison of LBDP with other approaches using (a) ARP, (b) ARR, (c) F-score and (d) ANMRR evaluation criteria over NEMA-CT.

Table 3. Results comparison of different methods in terms of ARP for $t\_m = 5$, ARR for $t\_m = 50$, F and ANMRR over NEMA-CT database

Performance	Method					
	LBP	LTP	PVEP	LTCoP	LMeP	LBDP
ARP (%)	99.34	99.10	98.84	98.95	98.90	99.55
ARR (%)	67.85	66.95	66.73	75.00	65.06	75.83
F (%)	59.11	55.72	58.42	65.12	57.59	67.64
ANMRR (%)	20.88	23.62	23.03	10.27	25.08	08.11

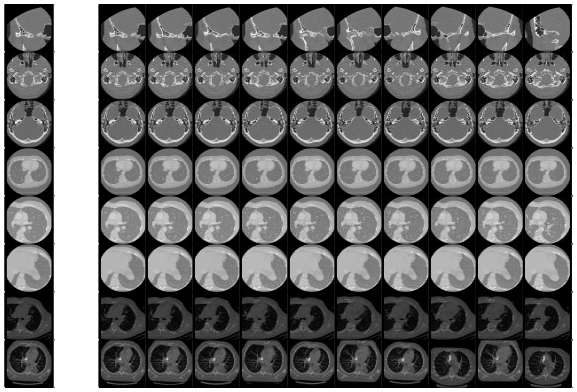

Fig. 11. Retrieved images in (b) by considering one query image in (a) from each category (one row for each) of the NEMA-CT database.

Fig. 10(a-d) depicts the performances of different methods using the ARP, ARR, F and ANMRR respectively as a function of the number of images retrieved. Table 3 lists the ARP values when $t\_m = 5$, ARR values when $t\_m = 50$, F values and ANMRR values in % for each method over NEMA-CT database. It can be seen that the ARP, ARR and F values for the proposed descriptor is highest while the ANMRR values for the proposed descriptor is lowest which points out the improved distinctive ability of the LBDP descriptor. The top 10 matching images (i.e. 10 most relevant retrieved images) are shown in the Fig. 11 for the 8 query images (one query from each class of the NEMA-CT database, see the Fig. 11(a)) using the proposed descriptor. In each case, the system is gained 100% precision as all the retrieved images are correct (see the Fig. 11(b)). Experimental results suggest that our approach is able to produce better retrieval performance as compared to the other approaches over NEMA-CT database.

C. *Experiment #3*

In this experiment, we considered a magnetic resonance imaging (MRI) database which is made public for research and analysis by the Open Access Series of Imaging Studies (OASIS) [40]. The cross-sectional images (resolution 176×208) of 421 persons are included in this database from the age-group between 18 and 96 years. We partitioned this database into four categories having 106, 89, 102 and 124 images for image retrieval uses on the basis of the ventricular shape inside the images. Fig. 12 depicts the example images (four images per category) from the OASIS-MRI database. Performance comparison among LBP, LTP, PVEP, LTCoP, LMeP and LBDP descriptor considering ARP vs t_m (Fig. 13(a)), Average Precision vs category (Fig. 13(b)), F vs t_m (Fig. 13(c)) and ANMRR vs t_m (Fig. 13(d)) are presented in Fig. 13 over OASIS-MRI database. The ARP using proposed LBDP method is increased by 30.58%, 27.98%, 22.65%,

23.67% and 27.27% of the ARPs using LBP, LTP, PVEP, LTCoP and LMeP methods respectively when $t\_m = 10$. The proposed method also performs better than other methods in each category of the OASIS-MRI database. The F value for proposed descriptor is second highest while the ANMRR value for proposed descriptor is lowest as compared to the other descriptors. The retrieval results over OASIS-MRI database confirm the superiority of LBDP.

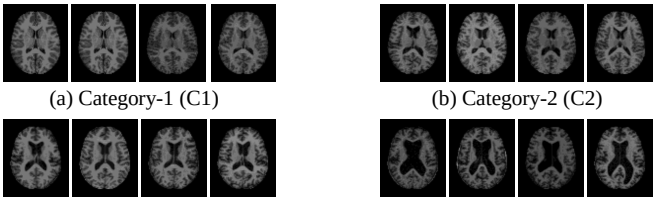

(a) Category-1 (C1) (b) Category-2 (C2)

(c) Category-3 (C3) (d) Category-4 (C4)

Fig. 12.OASIS-MRI example images, seven images from each group.

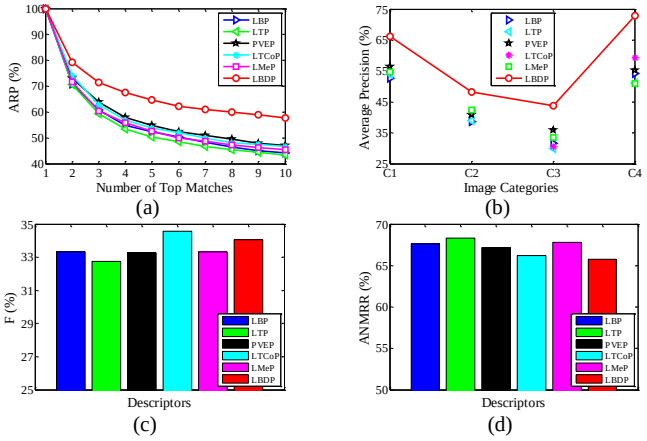

Fig. 13. Results in terms of the (a) ARP, (b) Average Precision per category, (c) F and (d) ANMRR over OASIS-MRI database.

Table 4. The total feature extraction time and total retrieval time in seconds over Emphysema-CT, NEMA-CT and OASIS-MRI databases using LBP, LTP, PVEP, LTCoP, LMeP and LBDP descriptors.

Descriptors	Total Feature Extraction Time			Total Retrieval Time		
	Emphysema-CT	NEMA-CT	OASIS-MRI	Emphysema-CT	NEMA-CT	OASIS-MRI
LBP	0.63	49.43	9.31	0.07	0.46	0.34
LTP	0.80	79.83	12.25	0.11	0.84	0.58
PVEP	3.45	623.56	74.36	1.45	12.63	9.56
LTCoP	1.15	241.79	22.20	0.11	0.85	0.61
LMeP	0.81	107.40	12.60	0.14	1.52	1.42
LBDP	2.39	606.20	56.78	0.06	0.43	0.33

D. Performance V/S Time Complexity

The total feature extraction time and total retrieval time in seconds is depicted in Table 4 using the proposed (i.e. LBDP) and other methods (i.e. LBP, LTP, PVEP, LTCoP and LMeP) over each database considering all the images (i.e. Emphysema-CT, NEMA-CT and OASIS-MRI). All the experiments are conducted using a system having Intel(R) Core(TM) i5 CPU 650@3.20 GHz processor, 4 GB RAM, and 32-bit Windows 7 Ultimate operating system. The feature extraction time of LBDP is only better than the PVEP over each database. It is obvious that the retrieval time of LBDP is nearly same as of LBP but it is much faster than other remaining methods over each database.

From the experimental results in terms of ARP, ARR, F-score, ANMRR and retrieval time obtained over Emphysema-CT, NEMA-CT and OASIS-MRI databases, it is evident that the proposed method are more discriminative and efficient than existing methods. We also analyzed that the performance of LBDP is nearly same under different settings of the number and radius of the local neighbors considered, whereas, its dimension doesn't change at all with these parameters.

V. Conclusion

A novel local bit-plane decoded pattern (LBDP) based image feature description is proposed in this paper for biomedical image indexing and retrieval. The LBDP transforms the local neighborhood in each plane and then encodes the relationship between the intensity value of centre pixel and transformed values to generate the LBDP binary pattern. The construction process of LBDP is different from the existing image feature descriptors. The dimension of the proposed method depends upon the bit depth of the image and also it is invariant to the number of local neighbors under consideration. Three biomedical image retrieval experiments were carried out to investigate the discriminative power and efficiency of LBDP in terms of the ARP, ARR, F-score and ANMRR. From the experimental results over two CT (Emphysema-CT and NEMA-CT) and one MRI (OASIS-MRI) database, it is confirmed that LBDP outperforms the recent state-of-art feature descriptors. The retrieval time using LBDP is reduced significantly while at the same time the performance is geared up. The LBDP feature description can also be utilized for invariant face recognition task.

References

[1] M.M. Rahman, S.K. Antani and G.R. Thoma, "A learning-based similarity fusion and filtering approach for biomedical image retrieval using SVM classification and relevance feedback", *IEEE Trans. Inf. Tech. Biomed.*, vol. 15, no. 4, pp. 640-646, 2011.

[2] H. Muller, A. Rosset, J.-P. Vallee and A. Geisbuhler, "Comparing feature sets for content-based image retrieval in a medical case database", Proc. *SPIE Med. Imag., PACS Imag. Inf.*, pp. 99 -109, 2004.

[3] L. Zheng, A.W. Wetzel, J. Gilbertson and M.J. Becich, "Design and analysis of a content-based pathology image retrieval system", *IEEE Trans. Inf. Tech. Biomed.*, vol. 7, no. 4, pp. 249-255, 2003.

[4] A. Quddus and O. Basir, "Semantic image retrieval in magnetic resonance brain volumes", *IEEE Trans. Inf. Tech. Biomed.*, vol. 16, no. 3, pp. 348-355, 2012.

[5] X. Xu, D.-J. Lee, S. Antani and L.R. Long, "A Spine X-Ray image retrieval system using partial shape matching", *IEEE Trans. Inf. Tech. Biomed.*, vol. 12, no. 1, pp. 100-108, 2008.

[6] H.C. Akakin and M.N. Gurcan, "Content-Based microscopic image retrieval system for multi-image queries", *IEEE Trans. Inf. Tech. Biomed.*, vol. 16, no. 4, pp. 758-769, 2012.

[7] G. Scott and C.-R. Shyu, "Knowledge-Driven multidimensional indexing structure for biomedical media database retrieval", *IEEE Trans. Inf. Tech. Biomed.*, vol. 11, no. 3, pp. 320-331, 2007.

[8] H. Muller, N. Michoux, D. Bandon and A. Geisbuhler, "A review of content-based image retrieval systems in medical applications - Clinical benefits and future directions", *J. Med. Inf.*, vol. 73, pp. 1-23, 2004.

[9] A.W.M. Smeulders, M. Worring, S. Santini, A. Gupta, and R. Jain, "Content-based image retrieval at the end of the early years," *IEEE Trans. PAMI*, vol. 22, no. 12, pp. 1349–1380, Dec. 2000.

[10] Y. Liu, D. Zhang, G. Lu, andW.-Y.Ma, "A survey of content-based image retrieval with high-level semantics," *Pattern Recog.*, vol. 40, pp. 262–282, 2007.

[11] T. Ojala, M. Pietikainen, and D. Harwood, "A comparative study of texture measures with classification based on feature distributions," *Pattern Recog.*, vol. 29, no. 1, pp. 51–59, 1996.

[12] T. Ojala, M. Pietikainen and T. Maenpaa, "Multiresolution gray-scale and rotation invariant texture classification with local binary patterns", *IEEE Trans. PAMI*, vol. 24, no. 7, pp. 971-987, 2002.
[13] F.S. Zakeri, H. Behnam and N. Ahmadinejad, "Classification of benign and malignant breast masses based on shape and texture features in sonography images", *J. Med. Syst.*, vol. 36, no. 3, pp. 1621-1627, 2012.
[14] G. Quellec, M. Lamard, G. Cazuguel, B. Cochener and C. Roux, "Wavelet optimization for content-based image retrieval in medical databases", *J. Med. Image Anal.*, vol. 14, pp. 227-241, 2010.
[15] A. Traina, C. Castanon and C. Traina Jr., "Multiwavemed: a system for medical image retrieval through wavelets transformations", Proc. *16th IEEE Symp. Comput.-Based Med. Syst.*, pp. 150 -155, 2003.
[16] J.C. Felipe, A.J.M. Traina and C. Traina Jr., "Retrieval by content of medical images using texture for tissue identification", Proc. *16th IEEE Symp. Comput.-Based Med. Syst.*, pp. 175-180, 2003.
[17] S. R. Dubey, S. K. Singh, and R. K. Singh, "Local Diagonal Extrema Pattern: A New and Efficient Feature Descriptor for CT Image Retrieval," *IEEE Signal Processing Letters*, vol. 22, no. 9, pp. 1215-1219, 2015.
[18] S. Murala and Q.M.J. Wu, "Local ternary co-occurrence patterns: A new feature descriptor for MRI and CT image retrieval", *Neurocomputing*, vol. 119, pp. 399-412, 2013.
[19] S. Murala, R.P. Maheshwari and R. Balasubramanian, "Directional binary wavelet patterns for biomedical image indexing and retrieval", *J. Med. Syst.*, vol. 36, no. 5, pp. 2865-2879, 2012.
[20] W. Cai, D.D. Feng and R. Fulton, "Content-based retrieval of dynamic PET functional images", *IEEE Trans. Inf. Tech. Biomed.*, vol. 4, no. 2, pp. 152-158, 2000.
[21] B. Zhang, Y. Gao, S. Zhao and J. Liu, "Local derivative pattern versus local binary pattern: Face recognition with higher-order local pattern descriptor", *IEEE Trans. Image Process.*, vol. 19, pp. 533-544, 2010.
[22] S. Liao, M.W.K. Law and A.C.S. Chung, "Dominant local binary patterns for texture classification", *IEEE Tans. Image Proc.*, vol. 18, no. 5, pp. 1107-1118, 2009.
[23] Z. Guo, L. Zhang and D. Zhang, "A completed modeling of local binary pattern operator for texture classification", *IEEE Tans. Image Proc.*, vol. 19, no. 6, pp. 1657-1663, 2010.
[24] T. Ahonen, A. Hadid and M. Pietikainen, "Face description with local binary patterns: Applications to face recognition", *IEEE Trans. Pattern Anal. Mach. Intell.*, vol. 28, no. 12, pp. 2037-2041, 2006.
[25] S. He, J.J. Soraghan, B.F. O'Reilly and D. Xing, "Quantitative analysis of facial paralysis using local binary patterns in biomedical videos", *IEEE Trans. Biomed. Eng.*, vol. 56, no. 7, pp. 1864-1870, 2009.
[26] L. Sorensen, S.B. Shaker and M. de Bruijne, "Quantitative analysis of pulmonary emphysema using local binary patterns", *IEEE Trans. Med. Imag.*, vol. 29, no. 2, pp. 559-569, 2010.
[27] X. Tan and B. Triggs, "Enhanced local texture feature sets for face recognition under difficult lighting conditions", *IEEE Trans. Image Process.*, vol. 19, no. 6, pp. 1635-1650, 2010.
[28] M. Heikkil, M. Pietikainen and C. Schmid, "Description of interest regions with local binary patterns", *Pattern Recog.*, vol. 42, pp. 425-436, 2009.
[29] S. R. Dubey, S. K. Singh, and R. K. Singh, "A multi-channel based illumination compensation mechanism for brightness invariant image retrieval," *Multimedia Tools and Applications*, 2014. DOI: 10.1007/s11042-014-2226-5.
[30] S. R. Dubey, S. K. Singh, and R. K. Singh, "Rotation and Illumination Invariant Interleaved Intensity Order Based Local Descriptor," *IEEE Transactions on Image Processing*, vol. 23, no. 12, pp. 5323-5333, 2014.
[31] S. Peng, D. Kim, S. Lee and M. Lim, "Texture feature extraction on uniformity estimation for local brightness and structure in chest CT images", *J. Compt. Biol. Med.*, vol. 40, pp. 931-942, 2010.
[32] D. Unay, A. Ekin and R.S. Jasinschi, "Local structure-based region-of-interest retrieval in brain MR images", *IEEE Trans. Inf. Tech. Biomed.*, vol. 14, no. 4, pp. 897-903, 2010.
[33] B. Li and M.Q.-H. Meng, "Tumor recognition in wireless capsule endoscopy images using textural features and SVM-Based feature selection", *IEEE Trans. Inf. Tech. Biomed.*, vol. 16, pp. 323-329, 2012.
[34] S. Murala and Q.M.J. Wu, "Local Mesh Patterns Versus Local Binary Patterns: Biomedical Image Indexing and Retrieval", *IEEE Journal of Biomedical and Health Informatics*, vol.18, no.3, pp. 929-938, 2014.
[35] S. Murala and Q.M.J. Wu, "Peak Valley Edge Patterns: A New Descriptor for Biomedical Image Indexing and Retrieval", Proc. *IEEE CVPR Workshops*, pp. 444-449, 2013.
[36] S. Murala and Q.M.J. Wu, "MRI and CT image indexing and retrieval using local mesh peak valley edge patterns", *Signal Processing: Image Communication*, vol. 29, no. 3, pp. 400–409, 2014.
[37] K. Lu, N. He, J. Xue, J. Dong, and L. Shao, "Learning View-Model Joint Relevance for 3D Object Retrieval", *IEEE Transactions on Image Processing*, vol. 24, no. 5, pp. 1449-1459, 2015.
[38] L. Sørensen, S. B. Shaker, and M. de Bruijne, "Quantitative Analysis of Pulmonary Emphysema using Local Binary Patterns," *IEEE Transactions on Medical Imaging*, vol. 29, no. 2, pp. 559-569, 2010.
[39] NEMA–CT image database. Available from [Online]: ⟨ftp://medical.nema.org/ medical/Dicom/Multiframe/⟩.
[40] D.S. Marcus, T.H. Wang, J. Parker, J.G. Csernansky, J.C. Morris and R.L. Buckner, "Open access series of imaging studies (OASIS): Crosssectional MRI data in young, middle aged, nondemented, and demented older adults", *J. Cogn. Neurosci.*, vol. 19, no. 9, pp. 1498-1507, 2007.
[41] P. Gravel, G. Beaudoin, and J. A. De Guise, "A method for modeling noise in medical images," *IEEE Transactions on Medical Imaging*, vol. 23, no. 10, pp. 1221-1232, 2004.